Quantitative Computed Tomography of Humpback Whale (*Megaptera novaeangliae*) Mandibles: Mechanical Implications for Rorqual Lunge-Feeding

DANIEL J. FIELD,[1*] REGINA CAMPBELL-MALONE,[2] JEREMY A. GOLDBOGEN,[1] AND ROBERT E. SHADWICK[1]

[1]Department of Zoology, University of British Columbia, Vancouver, British Columbia, Canada

[2]Biology Department, Woods Hole Oceanographic Institution, Woods Hole, Massachusetts

ABSTRACT

Rorqual whales (Balaenopteridae) lunge at high speed with mouth open to nearly 90 degrees to engulf large volumes of prey-laden water. This feeding process is enabled by extremely large skulls and mandibles that increase mouth area, thereby facilitating the flux of water into the mouth. When these mandibles are lowered during lunge-feeding, they are exposed to high drag, and therefore, may be subject to significant bending forces. We hypothesized that these mandibles exhibited a mechanical design (shape and density distribution) that enables these bones to accommodate high loads during lunge-feeding without exceeding their breaking strength. We used quantitative computed tomography (QCT) to determine the three-dimensional geometry and density distribution of a pair of subadult humpback whale (*Megaptera novaeangliae*) mandibles (length = 2.10 m). QCT data indicated highest bone density and cross-sectional area, and therefore, high resistance to bending and deflection, from the coronoid process to the middle of the dentary, which then decreased towards the anterior end of the mandible. These results differ from the caudorostral trends of increasing mandibular bone density in mammals, such as humans and the right whale, *Eubalaena glacialis*, indicating that adaptive bone remodeling is a significant contributing factor in establishing mandibular bone density distributions in rorquals. Anat Rec, 293:1240–1247, 2010. © 2010 Wiley-Liss, Inc.

Key words: rorqual; mandible; lunge-feeding; quantitative computed tomography; flexural rigidity

Cetacean bone, like that of all mammals, is a stiff structure composed of collagen, calcium hydroxyapatite, and water (Currey, 2002). Unlike the bones of other mammals, however, those of mysticetes are unique in that they display no clear-cut transition between cancellous and cortical bone, instead exhibiting a gradient of increasing density towards the bone's outer surface (Campbell-Malone, 2007). Mechanical function plays a significant role in mammalian bone remodeling, and may cause bone density to increase to ensure that there is enough bone tissue to withstand load-bearing (Lanyon, 1984). Cetaceans have an entirely aquatic existence,

Grant sponsor: NSERC undergraduate summer research award; Grant sponsor: NSERC discovery grant.

*Correspondence to: Daniel J. Field, 6270 University Blvd., Room 1316, Vancouver, British Columbia,V6T 1Z4, Canada
E-mail: danielf@interchange.uba.ca

Received 11 February 2010; Accepted 12 February 2010

DOI 10.1002/ar.21165

Published online 17 May 2010 in Wiley InterScience (www.interscience.wiley.com).

and therefore, are not subject to the same types of gravitational forces that a terrestrial mammal must contend with; however, cetaceans exhibit a wide range of complex behaviors that will impose dynamic loads on the musculoskeletal system.

Rorquals are a group of baleen whales (Mysticeti: Balaenopteridae) that include some of the largest animals of all time (Goldbogen et al., 2007). Balaenopterids are distinguished from other whales by a unique method of prey capture, known as "lunge-feeding." This method has been referred to as "the largest biomechanical action in the animal kingdom," and involves the whales engulfing a huge volume of prey-laden water (Brodie, 1993). During a lunge, rorquals approach dense swarms of prey at high speed, raise their heads and open their mouths by lowering their jaws (Lambertsen et al., 1995; Koolstra et al., 2004). The drag generated from an open mouth at high speed acts on the floor of the mouth, causing the elastic ventral groove blubber to expand up to several times its resting dimensions (Goldbogen et al., 2007; Orton and Brodie, 1987). These forces are such that the whale's kinetic energy is quickly lost during a lunge, greatly reducing the whale's speed (Goldbogen et al., 2006; Potvin et al., 2009). Although the basic mechanics of lunge-feeding are now relatively well-understood, the morphological specializations (especially with respect to the skull) required to execute a lunge are largely unknown.

Rorqual mandibles make up a large proportion of the body, nearly 25% of the whale's body length, and therefore, represent some of the longest bony elements to have ever existed. For example, the chord length of fin whale mandibles (*Balaenoptera musculus*) is known to approach 4.5 m in length (Lambertsen et al., 1995). Baleen whales are not known to masticate, and their two edentulous mandibles are each composed of a single bony element, the dentary. This bone consists of a bulbous posterior end comprising a dorsal condyle and ventral subcondylar process, and a long, slightly curved horizontal body (corpus). Instead of fusing at the mandibular symphysis, which is the case in other mammals, the rostral ends of the mandibles are separated by a dense fibrocartilage disc containing a "jelly-like" core (Brodie, 1993; Lambertsen et al., 1995; Pivorunas, 1977). The mandibular condyles of balaenopterids are completely embedded in a large connective tissue mass infiltrated with oil, referred to here as the temporomandibular joint (TMJ) pad, instead of being joined to the skull by a synovial joint as is seen in other mammals (Lambertsen, 1995; Brodie, 1993, 2001). These specialized fibrocartilage joints enhance the maneuverability of the mandibles, especially with respect to rotation (Lambertsen et al. 1995; Arnold et al., 2005), and facilitate the extreme gape angles that are observed during lunge-feeding (Brodie, 2001; Goldbogen et al., 2007).

The posterior end of the mandible is the attachment site of several muscles that depress and lift the jaws, opening and closing the mouth. These include the masseter, the depressor mandibularis, and the temporalis muscles (Schulte, 1916; Lambertsen, 1983; Lambertsen et al., 1995). Because of these muscle attachments, as well as the fact that the condyles are constrained by the TMJ pad to a certain extent, the mandibles should behave mechanically like a cantilever beam. The stresses encountered by a cantilever beam that is constrained at one end, and which experiences a uniform bending force along its length, will steadily increase towards the immobilized end of the beam. Therefore, we predicted the flexural rigidity of the mandibles to be greatest at their immobilized ends, immediately rostral to the TMJ pads, and to steadily decrease toward the anterior tips of the mandible. The flexural rigidity of an object is a product of material stiffness (the Young's modulus, E), determined by the mineral density, and the geometric arrangement of the material (the second moment of area, I). We predicted that both E and I of the mandibles would increase towards the mandibular condyles, to maximize the bones' flexural rigidity during a lunge-feeding event.

Although an analysis of the internal morphology and mechanics of balaenopterid mandibles has not been previously performed, the physical and material properties of the right whale jawbone (*Eubalaena glacialis*) have been investigated to obtain data contributing to a model of the stresses required to fracture the bone (Campbell-Malone, 2007; Tsukrov et al., 2009). This analysis yielded similar trends in posteroanterior density of the mandibles to those observed in humans (Campbell-Malone, 2007). Balaenids are not known to engulf large volumes of water, and instead have a flow-through filter with water entering the mouth and exiting through the baleen (Campbell-Malone, 2007; Werth, 2004; Simon et al., 2009). As such, the hydrodynamic stresses experienced by the balaenid mandible during feeding are different, and likely lower than those experienced by rorquals. Further, the balaenid mandible differs morphologically from that of rorquals by exhibiting a smaller and less laterally deviated coronoid process, a relatively larger mandibular condyle, and no TMJ pad (Campbell-Malone, 2007). This study attempts to determine if the divergent feeding mechanisms of rorquals and balaenids are associated with differing internal mandibular morphology.

MATERIALS AND METHODS

A sub adult female humpback whale (DFO 2408) was found dead and entangled in fishing gear on the British Columbia coast in May 2006. The whale's total body length was 8 m from the tip of the rostrum to the tail notch, which is approximately the observed length at weaning for this species (Huang et al., 2009). So, we assume that the animal was a lunge-feeder or was just starting to develop lunge-feeding behavior. Both mandibles were cleaned by being buried in horse manure for 12 months, and were subsequently lightly pressure washed. After preparation the dried skeleton was transported to the University of British Columbia for the ultimate goal of museum display. The left and right mandibles were subsequently scanned at the Vancouver General Hospital using a Siemens Somatom Definition dual energy CT scanner (Munich, Germany, http://www.medical.siemens.com).

Both mandibles were measured with a tape measure to obtain their straight length and external curved length. The straight length was defined as the distance between the anterior-most point of the body of the mandible and the posterior-most point of the condyles. The tape was held straight, above the bone surface. The external curved length was measured between the same two points; however, the tape measure was placed in

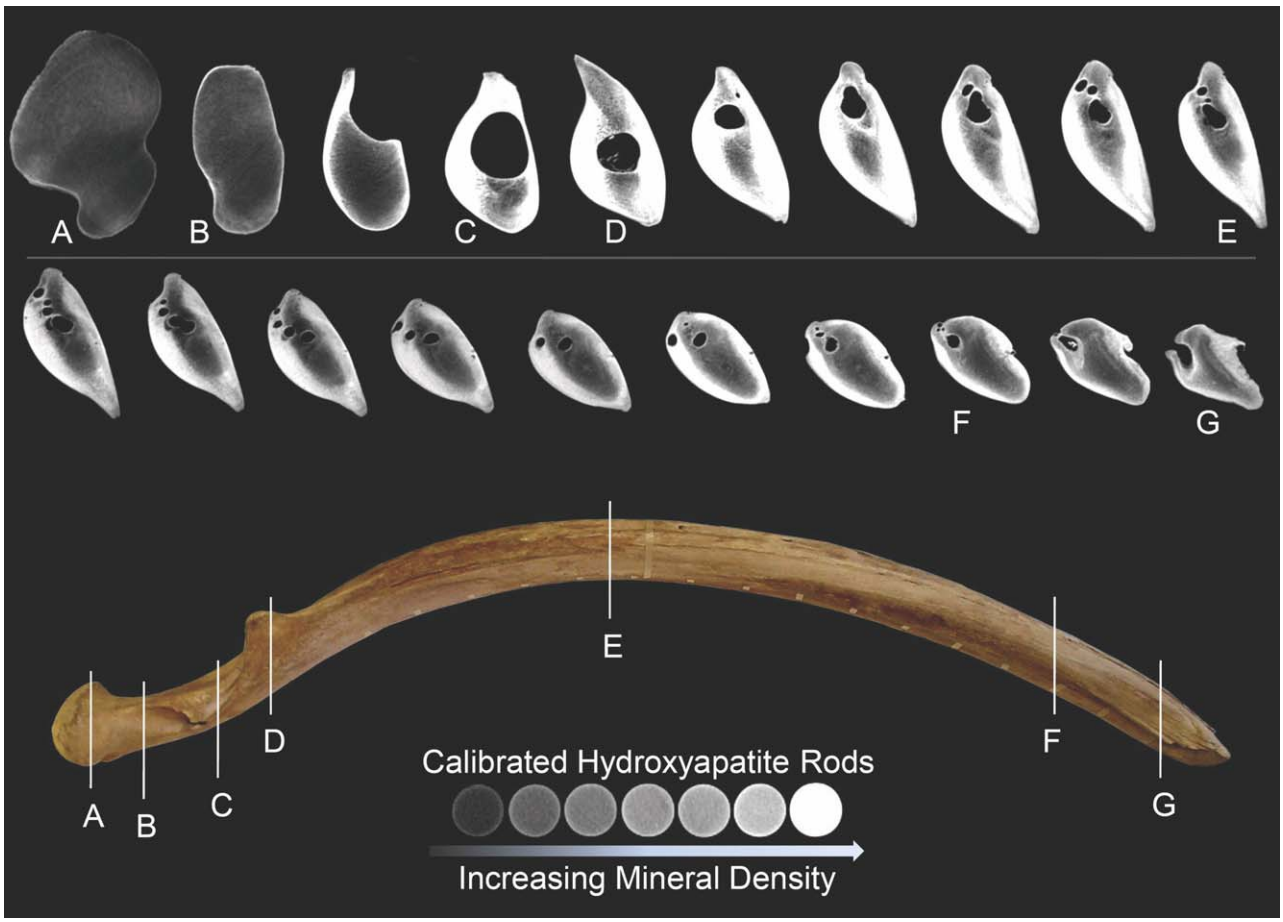

Fig. 1. QCT cross-sections through the left mandible of DFO 2408, beginning at the middle of the mandibular condyle (**A**), and proceeding rostrally. The dorsal surface of the mandible is up. The sections displayed are ~10 cm apart from one-another. Low-density bone appears gray on the CT scan, whereas high-density bone appears bright white. Air appears black. The position of sections **A**–**G** are shown through the left mandible of DFO 2408. From left to right, the hydroxyapatite rods displayed correspond to densities equivalent to water and 75, 200, 500, 800, 1000, and 1250 mg hydroxyapatite/cc.

contact with the middle of the mandible's medial surface. The definitions of straight length and external curved length, as well as the measuring methodology, are taken from Campbell-Malone (2007). The mandibles were also weighed with a digital scale accurate to 100 g.

Eleven hydroxyapatite standards, or "phantoms," of known mineral density were scanned under the same conditions as the mandibles. The mineral density of these standards is based on the amount of calcium hydroxyapatite suspended in the water-equivalent background when the standards were manufactured (Campbell-Malone, 2007). We used least-squares to determine the relationship between the Hounsfield units reported by our laboratory imaging software, and mineral density, reported in gHA/cc. Hounsfield values were obtained at six sites along each of the phantoms. Representative cross-sections of the mandibles and phantoms are illustrated in Fig. 1.

The length of the mandibles exceeded that which the scanner could accommodate, thus each jaw was scanned twice: once beginning at the rostral end, and once beginning at the caudal end. This resulted in a region in the middle of each mandible that was scanned twice, and the resulting redundant slices were eliminated during analysis. Slice thickness was 1 mm, which resulted in the creation of ~2010 slices per mandible. These were stored in stacks of high-resolution DICOM files. Every 10th slice beginning at the caudal-most slice through the mandibular condyle was analyzed.

The DICOM images of the left and right mandibles and phantoms were imported into ImageJ (NIH version 1.41o). Every stack was set to the same threshold settings, so that the brightness of the bone in each image was constant. Any holes visible within the bone due to the mandibular canal or any of its branches were selected from the slice and eliminated, ensuring that measurements reported only values for the bone tissue itself. ImageJ was used to measure the cross-sectional area and the average density of each slice. Values for mineral density were calculated from Hounsfield units using the aforementioned least squares equation, and a similar equation was derived to convert the area measurements from ImageJ pixels to mm^2. We divided the mandible into four conceptual functional regions for comparative purposes, based on distinct anatomical features as described by Lambertsen et al. (1995): The

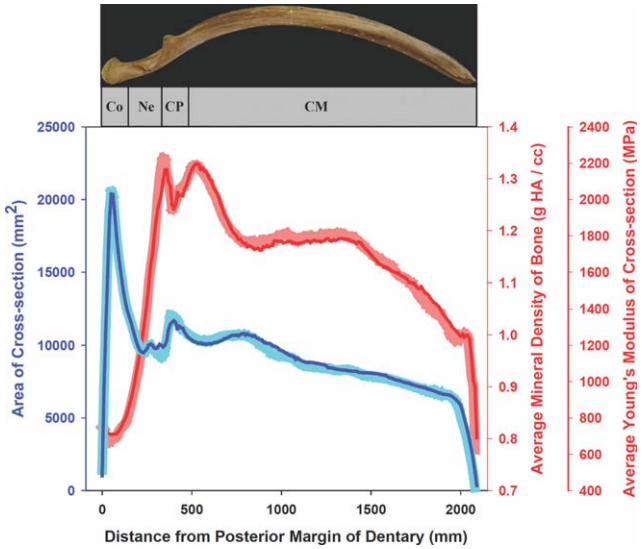

Fig. 2. Caudorostral trends in mandibular cross-sectional area, mean cross-sectional mineral density, and mean cross-sectional Young's modulus (given in MPa). The light and dark blue traces represent the caudorostral trends in cross-sectional area through the left and right mandibles of DFO 2408, respectively. The light and dark red traces represent the caudorostral trends in mineral density and Young's modulus through the left and right mandibles of DFO 2408, respectively. Co, Ne, CP, and CM show the portion of the mandibles encompassing the condyle, the neck, the region including the coronoid process, and the corpus mandibulae rostral to the coronoid process, respectively.

mandibular condyle, the "neck", the coronoid process region, and the corpus mandibulae. The positions of these regions are illustrated in Fig. 2.

Several regression equations have been derived, which relate noninvasive measurements of bone density [Hounsfield units, quantitative computed tomography (QCT) apparent density, etc.] to experimentally derived values of Young's modulus. This is possible because mineral density is the primary determinant of Young's modulus in bone (Currey, 2002). Campbell-Malone et al. (2007) tested the accuracy of several of these equations in predicting the Young's modulus of right whale mandibular bone, and determined that the most precise conversion was that derived by Ciarelli et al. (1991) (Campbell-Malone et al., 2007). Because of the importance of conserving our museum-quality specimens, we used this general regression equation, which relates the Hounsfield units from a CT scan (*H.U.*) to estimated Young's modulus (*E*est in MPa), rather than conducting destructive mechanical tests. Due to the anisotropy of the bone material tested in previous experiments (human femora, humeri, radii, and right whale mandibles), a regression equation was used to relate *H.U.* to the average Young's modulus for all three orthogonal directions (Ciarelli et al., 1991; Campbell-Malone, 2007):

$$E_{\text{est}} = -38.644 + 1.3665 \times (H.U) \quad (1)$$

The second moment of area (*I*) is a geometrical factor that takes into account the distribution of mass within the cross-section of a beam, and is important in the analysis of bending behavior. (Vogel, 2003). We examined *I* for selected cross-sections using the ImageJ plugin MomentMacroJ, v1.2. This plugin enabled the estimation of the maximum second moment of area and the location of a cross-section's centroid, as well as the principal axis (the axis along which the maximum second moment of area is located). The orientation of the principal axis was used to infer the direction of the maximum bending moment. This inference was compared with anatomical and functional knowledge of the balaenopterid craniomandibular apparatus to assess its validity.

RESULTS

The straight length of the right mandible of humpback whale DFO 2408 measured 2.1 m, and had a mass of 18.28 kg. The left mandible had a straight length of 2.07 m with a mass of 18.25 kg. The straight length to total body length ratio of this whale (~26.25%) falls within the range of values observed for other large whales (Campbell-Malone, 2007). The caudorostral trends in average bone mineral density, Young's modulus, and cross-sectional area throughout both jaws are shown in Fig. 2. A regression equation was used to relate the average density of a cross-section in Hounsfield units to an estimate of each cross-section's average Young's modulus (*E*). The average bone density and average Young's modulus of cross-sections increase from the rostral to the caudal end of the mandible, and are low through the mandibular condyle. These parameters also show a decrease at the coronoid process. The cross-sectional area of the mandible also increases from the rostral to the caudal end of the mandible, with the maximum cross-sectional area being located through the mandibular condyle.

The densities of eight cross-sections that included the coronoid process were analyzed with and without the coronoid process included in the scan. This enabled the estimation of the coronoid process's contribution to the slice's mean density. Depending on the cross-section, the coronoid process's presence resulted in a range of 1%–6 % decrease in cross-sectional mean density. The mean density for each functional region of the right mandible, as well as the mean density in the coronoid region with and without the coronoid, is displayed with 95% confidence intervals in Fig. 3. The mandibular condyle's mean density is significantly lower than any other functional region of the mandible. The mean density of the corpus mandibulae and the neck are significantly lower than the mean density of the coronoid process region.

The estimated orientations of the second moment of area's principal and neutral axes were determined for randomly selected cross-sections through the humpback whale's right mandible, with slices analyzed from all four functional regions. The principal axes caudal to the coronoid process were oriented dorsoventrally, and gradually became mediolaterally elongated towards the rostral end of the mandible.

DISCUSSION

Density Trends and Their Implications

The caudorostral trends in mandibular bone density reported by Campbell-Malone (2007) indicate a significant trend of increasing bone density towards the

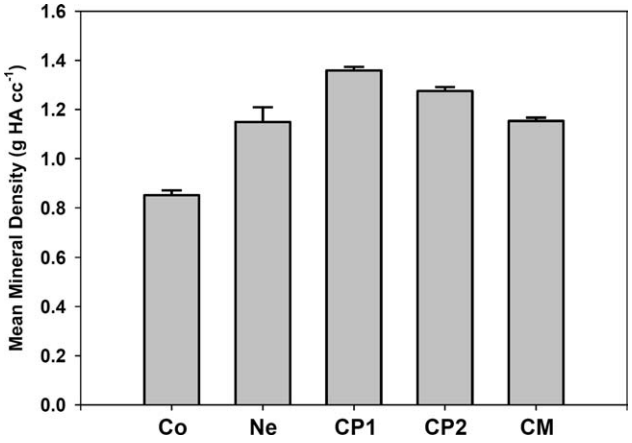

Fig. 3. Mean densities of the functional regions of the right mandible of DFO 2408. Co = condyle; Ne = neck; CP1 = coronoid region with coronoid process digitally removed, CP2 = coronoid region with coronoid process included, CM = corpus mandibulae rostral to the coronoid process. Ninety-five percentage confidence intervals are shown.

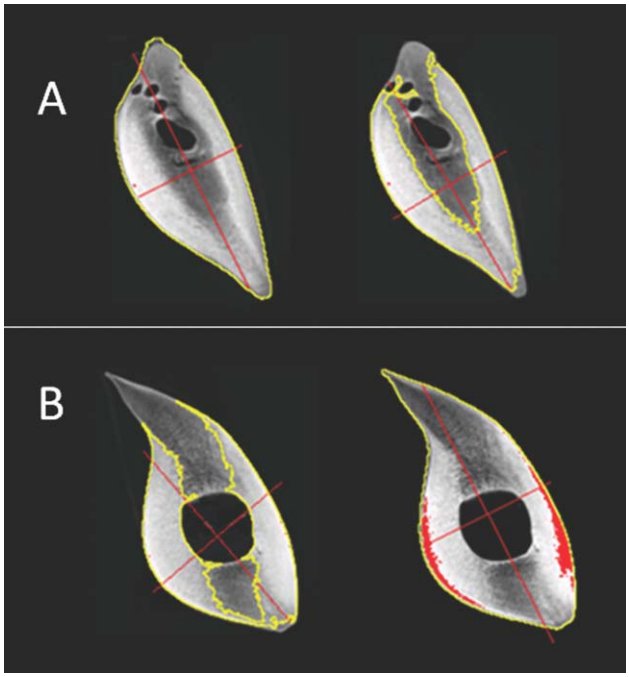

Fig. 4. Orientation of the principal axis of *I*, the second moment of area, through the middle of the corpus mandibulae (**A**), and the coronoid process (**B**) of the left mandible of DFO 2408. The longer red line represents the orientation of the principal axis, and the yellow outline indicates the region of bone analyzed to make this estimation. The centroid lies at the intersection of the two red lines. The pattern shown in A reflects that observed throughout the majority of the mandible, with the exclusive analysis of high-density bone causing only a minor skew of the estimation of the centroid's position, and virtually no difference in the orientation of the principal axis of *I*. The pronounced difference in orientation observed in B is because of the low-density bone of the coronoid process, which skews the estimation of the principal axis orientation when it is included. This is the only region exhibiting a pronounced difference in principal axis orientation when high-density bone is exclusively analyzed.

rostral end of the mandibles of North Atlantic right whales. The same trend is observed in the human mandible as well, a bone, that in addition to being extremely morphologically dissimilar, is morphologically designed for mastication (Misch et al., 1999). The fact that similar trends in caudorostral mandibular density are reported in an edentulous filter feeder-like the right whale and a masticating feeder-like humans suggests that caudorostral trends in mandibular bone density may reflect conservative developmental control of the mandible, similar to the conservative ontogenetic control of limb buds observed in a wide range of vertebrates (Campbell-Malone, 2007; Gilbert, 1997; von Dassow and Munro, 1999). Such developmental control may overshadow the possible role of functional remodeling as a morphological determinant. If the effects of dynamic mandibular bone remodeling in response to function are truly overshadowed by conservative mammalian developmental control, we would predict that rorquals would exhibit similar trends in caudorostral mandibular density to humans and right whales. However, as reported in Fig. 2, the mandible of *M. novaeangliae* exhibits a clearly discernible trend of decreasing mineral density from the condylar end to the rostral tip. We propose that this trend is a result of adaptive bone remodeling in response to applied stresses during feeding.

Mysticete mandibles contain a significant amount of intertrabecular fat *in vivo*; however, the treatment process removed nearly all of the fat from the mandibles analyzed in this study. Calibrated mineral content can lead to statistical error when fat is present (Campbell-Malone, 2007). This error can be as high as −10 mg/mL per 10% fat by volume (Laval-Jeantet et al., 1986). Campbell-Malone (2007) investigated right whale mandibles that had not been defatted, which would have affected the reported QCT bone density. Therefore, the trends in mineral density reported herein for the humpback mandible are comparable with those reported for the right whale by Campbell-Malone (2007), but the absolute mineral density values are not.

The classic example of a cantilever beam provides a suitable analogy for our interpretation of the function of balaenopterid mandibles during lunge-feeding, and may help explain the density distribution observed in the mandibles of *M. novaeangliae*. One may think of the drag force acting on mandibles during feeding as analogous to a force distributed uniformly along the length of a cantilever beam, which is essentially immobilized at one end. The tensile and compressive forces experienced by the beam will increase with distance outward from the neutral plane running down the beam's horizontal midline, and forces will steadily increase towards the immobilized end of the beam, the site of support from the load (Vogel, 2003). For example, a ruler clamped at one end that experiences a uniform bending force along its free end will break at the clamp, as the tensile and compressive forces are greatest there.

The balaenopterid mandible is anchored to the skull by the fibrous TMJ pad and by several muscles (most notably the temporalis, the masseter profunda and the masseter superficialis). All of these attachments are located at the posterior end of the mandible, and form the mandible's support from the load encountered during

feeding. The condylar ends of the mandibles are completely surrounded by the large TMJ pads, which may constrain the motion of the mandibular condyles, as well as the portion of the neck just rostral to the condyles (Lambertsen et al., 1995). It would be expected, therefore, that the bending stresses experienced by the mandible during a lunge-feeding event would increase steadily towards the fixed end of the mandible. For these reasons, we attribute the caudorostral trends in the humpback whale mandible's mineral density to adaptive bone remodeling in response to applied stress during lunge-feeding.

As Fig. 3 indicates, the mean density of the mandibular condyles, as well as the area of the neck just rostral to them, is significantly lower than any other region of the mandibles. The low mean mineral density of the condyles is probably due to lower bending forces relative to those experienced by the rest of the mandible, as they are essentially anchored by their position within the TMJ pad. That being stated, the rigidity of the condyle is in fact higher than would be indicated by their low mineral density, because the maximum cross-sectional area through the condyle is nearly twice that of the greatest cross-sectional area anywhere else on the mandible.

As flexural rigidity is both a function of a material's Young's modulus (E), and its geometrical arrangement (I), the area of the cross-section must also be considered as an important contributor to stiffness (Vogel, 2003). The extremely low mineral density of the mandibular condyle may be due to efficient damping of impulsive loads by the TMJ pad, which is essentially a flexible joint with enhanced volume (see Currey, 2002). The caudal portion of the neck is also surrounded by the rostralmost extension of the TMJ pads. This fact likely explains the huge increase in bone density from the caudal end of the neck to the rostral end (Fig. 2). As well, it is likely responsible for the fact that the mean bone density of the neck is significantly lower than the coronoid process region, as shown in Fig. 3. Similarly, the anterior tips of the mandibles were also very low in density, and they too are joined at the mandibular symphysis by a large fibrous mass that has been likened to an intervertebral disc (Pivorunas, 1977). Both the TMJ pad and the mandibular symphysis appear well-designed to accommodate the large excursions and shearing loads that may occur during lunge-feeding.

These observations provide support for the hypothesis that dynamic tissue remodeling is an important determinant of caudorostral mandibular density trends in *M. novaeangliae*. Either the forces incurred by the jaws of right whales and humans during feeding are insufficient to cause the bone to remodel enough to obscure the underlying conservative development of the mandible, or the remodeling of the bone in response to the forces experienced by the jaws during feeding is in fact responsible for the observed density distribution. The latter suggests that the similarity between the caudorostral density distribution found in humans and right whales mandibles is purely coincidental, and is most probable in our opinion. Further comparative studies of the density distributions of mammalian mandibular bone tissue are required to differentiate between these two potential explanations.

Notes on the Coronoid Process

A "dip" in bone density can be observed in Fig. 2, in the region that includes the coronoid process. This dip is due to decreased mineralization of the coronoid process relative to the body of the mandible. The low density of the coronoid process itself relative to the body of the mandible was surprising because previous studies indicated that the coronoid process is the primary site of attachment of the temporalis (Brodie, 2001; Lambertsen et al., 1995). This muscle presumably functions to lift the jaw and close the mouth after a lunge-feeding event. One possible explanation for these results is that the temporalis may attach to a greater area of the mandible than had been previously reported. In doing so, muscle force would be distributed over greater area of the bone and increase mechanical advantage. Lambertsen et al. (1995) provided a brief account of the temporalis's attachment to the region of the mandible surrounding the coronoid in balaenopterids. The authors indicated that the fibrous sheath surrounding the temporalis attaches primarily to the coronoid process, as well as maintaining lesser secondary attachments to the regions anterior and posterior to the coronoid.

Second Moment of Area and its Implications

The second moment of area (I) of a cross-section is a function of its shape. I is proportional to the square of the distance from an object's neutral axis, therefore an irregularly shaped object will have different values of I depending on the axis along which I is measured. The balaenopterid mandible is roughly elliptical in cross-section (Fig. 1), therefore, the maximum value of I will tend to be oriented along the axis of maximum cross-sectional distance. To resist bending one would expect the maximum value of a mandibular cross-section's I to occur along the same axis as the bending force acting on the mandible.

The calculation of I is based on the assumption that the object under investigation has a homogeneous material distribution, and as the mandibular bone tissue of *M. novaeangliae* varies considerably in density within individual cross-sections, a precise mathematical determination of the centroid, as well as values of I in various directions, was not attempted in this study. Therefore, we treated the concept of second moment of area only qualitatively, and our discussion of the subject is most applicable only in the relative sense.

Cross-sections through the mandible exhibited areas of widely different mineral density. To determine whether the inclusion of regions of low-density bone skewed our estimation of the second moment of area's principal axis, we compared the orientation of the axis when high-density bone was exclusively analyzed with the orientation when the entire cross-section was used (Fig. 4). This was accomplished by varying the contrast threshold in the image. This method yielded differences in principal axis orientation of only a few degrees. The only region exhibiting a marked difference in principal axis orientation during this comparison was the region encompassing the coronoid process. Here, when low-density bone was included in the calculation, the principal axis included a portion of the coronoid process. However, when high-density bone was exclusively selected, the

axis again became orientated dorsoventrally, similar to the orientation at other sites caudal to the coronoid. This difference was due to the coronoid process being composed of porous bone. It is possible that the increased second moment of area along the coronoid process may help provide flexural rigidity against the forces imposed upon it by the temporalis during mouth closure.

Caudal to the coronoid process, cross sections exhibited principal axes oriented dorsoventrally. This arrangement appears to be optimized for resisting dorsoventral bending forces during lunge-feeding. However, rostral to the coronoid process, the principal axes gradually became oriented more mediolaterally. This change in principal axis orientation accompanies the hypothetical decrease in bending forces from the caudal to the rostral end of the mandible. It is possible that the changing principal axis orientation of cross-sections along the mandible optimizes resistance to other forces that the mandible may be subject to, such as torsional stresses. However, because of the inaccuracy of modeling torsional stresses directly from non-cylindrical cross-sectional images, an analysis of the torsional stresses along the rorqual mandible during lunge-feeding was not attempted here (Daegling, 2002). Future finite element modeling of the mandibles will permit a quantitative analysis of the torsional stresses associated with lunge-feeding to be undertaken.

Trends in Cross-Sectional Area

Along most of the mandible, the caudorostral trends in mandibular cross-sectional area are parallel to those observed for mineral density. The cross-sectional area of the mandibles decreases steadily from the coronoid process into a tapering, narrow rostral tip. However, local maxima in cross-sectional area are observed at the coronoid of each mandible, which corresponds directly to local minima in apparent density (see "CP" region in Fig. 2). The portions of the mandibles exhibiting the greatest cross-sectional area are the mandibular condyles, which exhibit a markedly lower mean density than the remainder of the mandibles.

Our contention that the flexural rigidity of the mandibles decreases anteriorly is strengthened when the caudorostral trends in mandibular cross-sectional area are included in the analysis. It is evident that rostral to the coronoid process, the mandibles exhibit an overall trend of decreasing cross-sectional area. This reduces the magnitude of the second moment of area anteriorly, which combined with the decrease in Young's modulus observed in this area, makes the rostral ends of the mandibles relatively less resistant to bending forces.

CONCLUSIONS

Our analysis suggests that humpback whale mandibles exhibit a morphological design (mineral density distribution and shape) that is optimized for resisting the bending forces encountered during lunge-feeding. Although our study was limited to one specimen, these data provide valuable insight into the morphological specializations that facilitate lunge-feeding in rorquals. However, more studies are clearly necessary to adequately test the hypotheses presented herein. Ideally, multiple adult, or at least older juvenile specimens both within and among rorqual species should be analyzed to determine the variance in mandibular density distribution and shape. Furthermore, mechanical testing of fresh rorqual bone is needed to validate our QCT-derived values of E, which may be a possibility in the future if further specimens are obtained.

Our inferences regarding the relationship between the form and function of rorqual mandibles will be explicitly tested in the future using finite element modeling, which is currently underway. This study represents a necessary first step in the construction of such a model. A future comparative study examining the mandibles of other lunge-feeders is also in its formative stages, to evaluate our predictions regarding the cause of the observed density distribution throughout the mandibles of *M. novaeangliae*.

ACKNOWLEDGMENTS

The authors benefited from helpful discussions with Micha Ben-Zvi, Sheldon Pinto, John Gosline, Callum Ross, and Emily Rayfield. Comments on the manuscript from Wayne Vogl and two anonymous reviewers significantly improved this work. As well, the authors wish to thank Michael DeRoos, Morgan Davies, and Andrew Trites for providing access to the mandibles of DFO 2408, and Lisa Spaven for providing stranding information. John Mayo assisted with the CT scanning process.

LITERATURE CITED

Arnold PW, Birtles RA, Sobtzick S, Matthews M, Dunstan A. 2005. Gulping behavior in rorqual whales: underwater observations and function interpretation. Memoir Queensl Mus 51:309–332.

Brodie PF. 1993. Noise generated by the jaw actions of feeding fin whales. Can J Zool 71:2546–2550.

Brodie PK. 2001. Feeding mechanisms of rorquals (Balaenoptera sp.). In: Mazin J-M, de Buffrenil V, editors. Secondary adaptations of Tetrapods to life in water. Munchen, Germany: Verlag Dr. Friedrich Pfeil. p 345–352.

Campbell-Malone R. 2007. Biomechanics of north atlantic right whale bone: mandibular fracture as a fatal endpoint for blunt vessel-whale collision modeling, Doctoral Thesis in Biological Oceanography. Massachusetts Institute of Technology/Woods Hole Oceanographic Institution, Cambridge, MA. p 257.

Ciarelli MJ, Goldstein SA, Kuhn JL, Cody DD, Brown, MB. 1991. Evaluation of orthogonal mechanical properties and density of human trabecular bone from the major metaphyseal regions with materials testing and computed tomography. J Orthop Res 9, p 674–682.

Currey JD. 2002. Bones: structure and mechanics. Princeton, NJ: Princeton University Press. p 436.

Daegling DJ. 2002. Estimation of torsional rigidity in primate long bones. J Human Evol 43:229–239.

Gilbert SF. 1997. Development of the tetrapod limb. In: Gilbert, SF, editor. Developmental Biology Sinauear Associates, Inc.: Sunderland, Massachusetts. p 701–731, Chapter 18.

Goldbogen JA, Calambokidis J, Shadwick RE, Oleson EM, McDonald MA, Hildebrand JA. 2006. Kinematics of foraging dives and lunge-feeding in fin whales. J Exp Biol 209:1231–1244.

Goldbogen JA, Pyenson ND, Shadwick RE. 2007. Big gulps require high drag for fin whale lunge feeding. Marine Ecol Prog Ser 349: 289–301.

Huang SL, Chou LS, Ni IH. Comparable length at weaning in cetaceans. Marine Mammal Sci; Doi: 10.1111/j.1748-7692.2009.00288.x.

Koolstra JH, van Eijden TMGJ. 2004. Functional significance of the coupling between head and jaw movements. J Biomech 37: 1387–1392.

Lambertsen RH. 1983. Internal mechanism of rorqual feeding. J Mammal 64:76–88.

Lambertsen RH, Ulrich N, Straley J. 1995. Frontomandibular stay of Balaenopteridae: a mechanism for momentum recapture during feeding. J Mammal 76:877–899.

Lanyon LE. 1984. Functional strain as a determinant for bone remodeling. Calcified Tissue Int 36:56–61.

Laval-Jeantet AM, Roger B, Bouysee S, Bergot C, Mazess RB. 1986. Influence of vertebral fat content on quantitative CT density. Radiology 159:463–466.

Misch CE, Qu Z, Bidez MW. 1999. Mechanical properties of trabecular bone in the human mandible: implications for dental implant treatment planning and surgical placement. J Oral Maxillofacial Surg 57:700–706.

Orton LS, Brodie PF. 1987. Engulfing mechanics of fin whales. Can J Zool 65:2898–2907.

Perrin W, Wursig B, Thewissen JGM. 2002. Encyclopedia of marine mammals. Academic Press: Boston. p 1414.

Pivorunas A. 1977. The fibrocartilage skeleton and related structures of the ventral pouch of balaenopterid whales. J Morphol 151:299–313.

Potvin J, Goldbogen JA, Shadwick RE. Passive versus active engulfment: verdict from trajectory simulations of lunge-feeding fin whales *Balaenoptera physalus*. J Royal Soc Interface 6:1005–1025.

Schulte HVW. 1916. Anatomy of a foetus, *Balaenoptera borealis*. Memoir Am Mus Nat History 6:389–502.

Simon M, Johnson M, Tyack P, Madsen PT. Behaviour and kinematics of continuous ramfiltration in bowhead whales (*Balaena mysticetus*). Proc Royal Soc B: Biol Sci 276:3819–3828.

Tsukrov I, DeCew JC, Baldwin K, Campbell-Malone R, Moore MJ. 2009. Mechanics of the right whale mandible: full scale testing and finite element analysis. J Exp Marine Biol Ecol 374:93–103.

Vogel S. 2003. Comparative Biomechanics. Princeton, NJ: Princeton University Press, p 365–373.

von Dassow G, Munro E. 1999. Modularity in animal development and evolution: elements of a conceptual framework for EvoDevo. J Exp Zool 285:307–325.

Werth AJ. 2004. Models of hydrodynamic flow in the bowhead whale filter feeding apparatus. J Exp Biol 207:3569–3580.